Supplemental material

Hagiwara et al., https://doi.org/10.1083/jcb.201704076

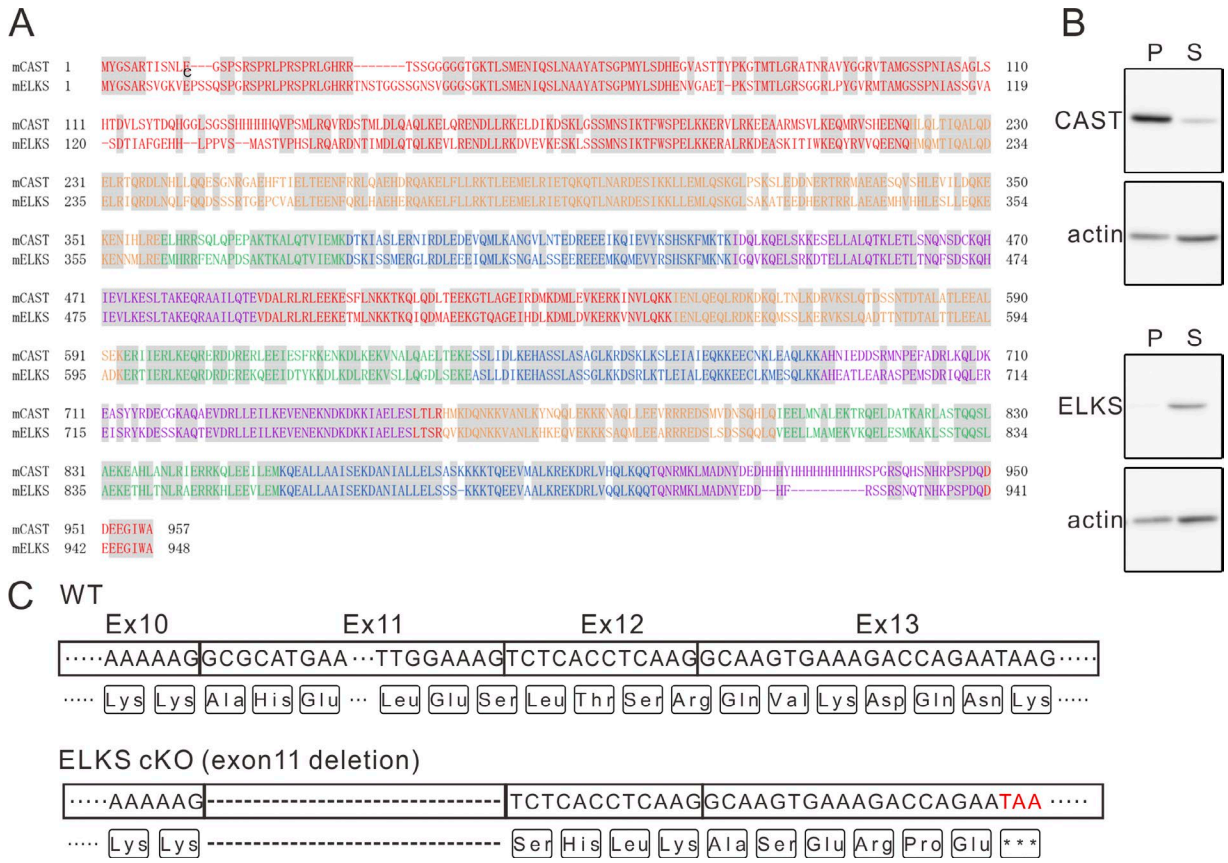

Figure S1. **Generation of ELKS flox strain, and Crx-Cre mediated ELKS cKO. (A)** Aligned amino acid sequence of mouse CAST and ELKS. Different colors indicated the amino acids from different exons. Corresponding sequences were indicated in gray boxes. These two proteins showed 71% identity and 92% similarity. **(B)** Comparison of CAST and ELKS protein solubility. Proteins expressed in COS7 cells were extracted with Triton X-100 and then separated into the pellet (P) and soluble (S) fractions. Almost 95% of ELKS was in the soluble fraction, while CAST was resistant to solubilization (<10%) by Triton X-100. **(C)** Deletion of Ex11 induced a frameshift mutation. The upper code indicates the DNA sequence in each exon, and the bottom shows the amino acids. Since nucleotides in Ex11 could not be divided by three, exposure to Cre recombinase caused an open reading frameshift. Different proteins were encoded downstream of the deletion site, and terminated by a stop codon (TAA in red).

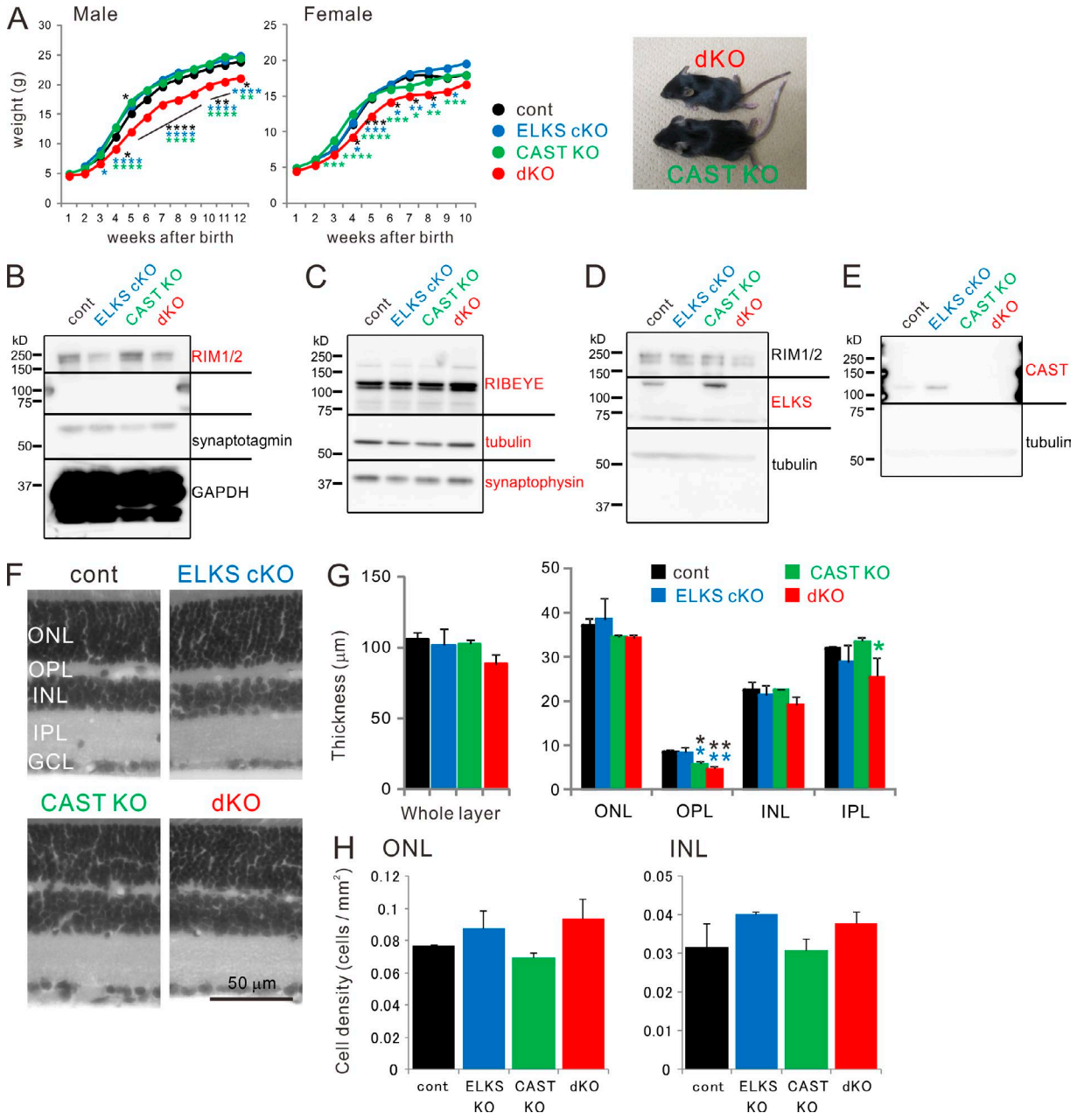

Figure S2. **Crx-Cre–mediated ELKS cKO and CAST/ELKS dKO mice in retina. (A)** Growth curve of Crx-Cre–mediated ELKS deletion mutants. The mutant mice were healthy and fertile. However, the dKO mice, especially males, could be identified with their smaller size (left), and the growth curve of mean body weight (SEM not shown for clarity) was significantly decreased from other genotypes. Colored asterisks, illustrating statistical comparison to the respectively colored genotypes, indicate statistical significance. *, P < 0.05; **, P < 0.01; ***, P < 0.001; ****, P < 0.0001 (two-way ANOVA followed by post hoc Bonferroni). **(B–E)** Original data from immunoblotting of adult (9–12-wk-old) retinal homogenates of mutant mice. The results for the antibodies indicated in red are shown in Fig. 1. The protein transferred membranes were split at the black lines for each antibody reaction, and then spliced together to detect luminescence. **(F–H)** Formation of layers in adult retina (~10 wk old) was analyzed in mutant mice. The thickness of OPL and IPL was reduced in the dKO mice. Fixed eyes were embedded in paraffin, and sections were stained with hematoxylin and eosin. The thickness of retina from ONL to ganglion cell layer (GCL) was slightly reduced in dKO. In detail, the thickness of OPL was reduced in CAST KO and dKO compared with the control and ELKS cKO, but difference between CAST KO and dKO was not significant. On the other hand, IPL was significantly reduced in dKO compared to the CAST KO (G). Cell densities in ONL and INL were not significantly different (H). *n* = 3 animals from each genotype; mean ± SEM. *, P < 0.05; **, P < 0.01 (one-way ANOVA followed by post hoc Tukey).

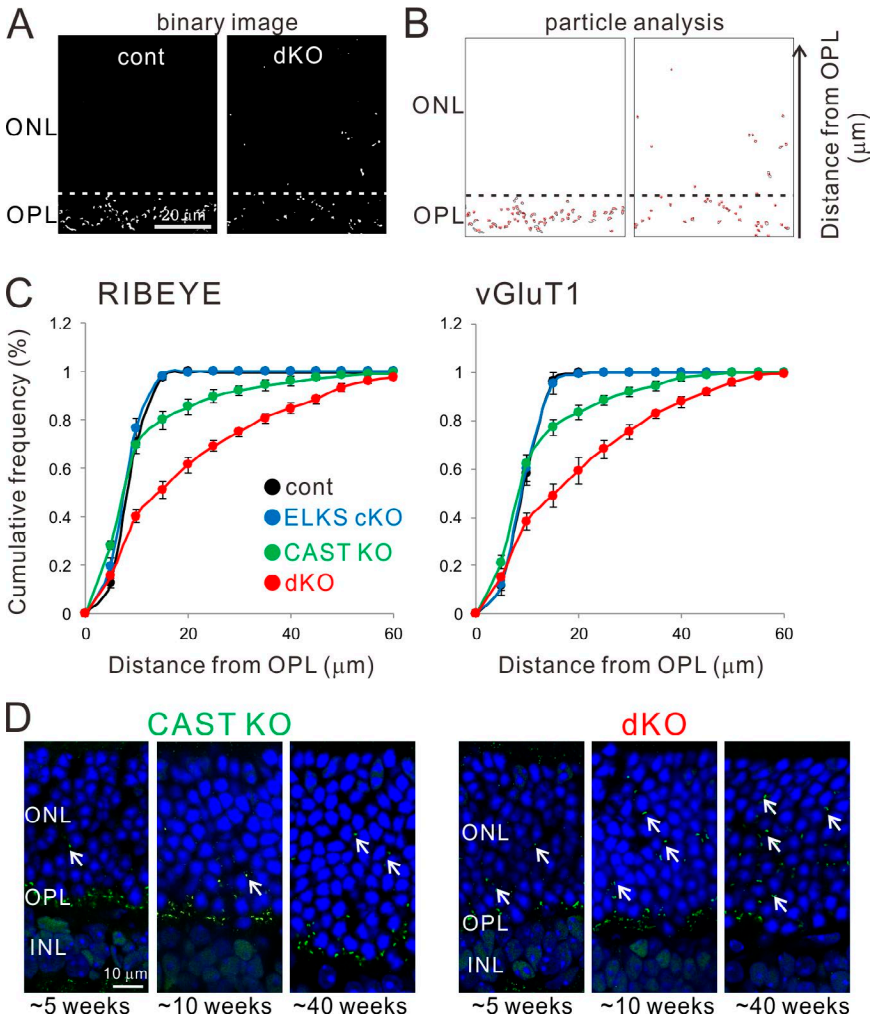

Figure S3. **Crx-Cre–mediated ELKS cKO and CAST/ELKS dKO mice in retina. (A and B)** To measure RIBEYE-immunolabeled ribbon synapse distribution from OPL to ONL, fluorescence images were transformed into binary images (A, cont and dKO), and particle distribution is shown in the y axis as the distance from the bottom of OPL, using the ImageJ analyze particle program (B). **(C)** Retinal sections were immunolabeled with RIBEYE and vGluT1 simultaneously, and then the distance probability was analyzed in the same area. The histograms of both RIBEYE and vGluT1 demonstrated enhanced ectopic synapses in CAST KO and dKO mice; mean ± SEM. **(D)** Representative images of enhanced ectopic synapses with age. In CAST KO, ectopic synapses were identified in 5- and 10-wk-old retinae, and the ectopic distribution at 40 wk is significantly increased. Furthermore, many ectopic synapses are detected even at 5 and 10 wk of age in dKO. Ectopic synapses are further increased at 40 wk, indicating age-dependent increased ectopic formation in CAST KO and dKO.

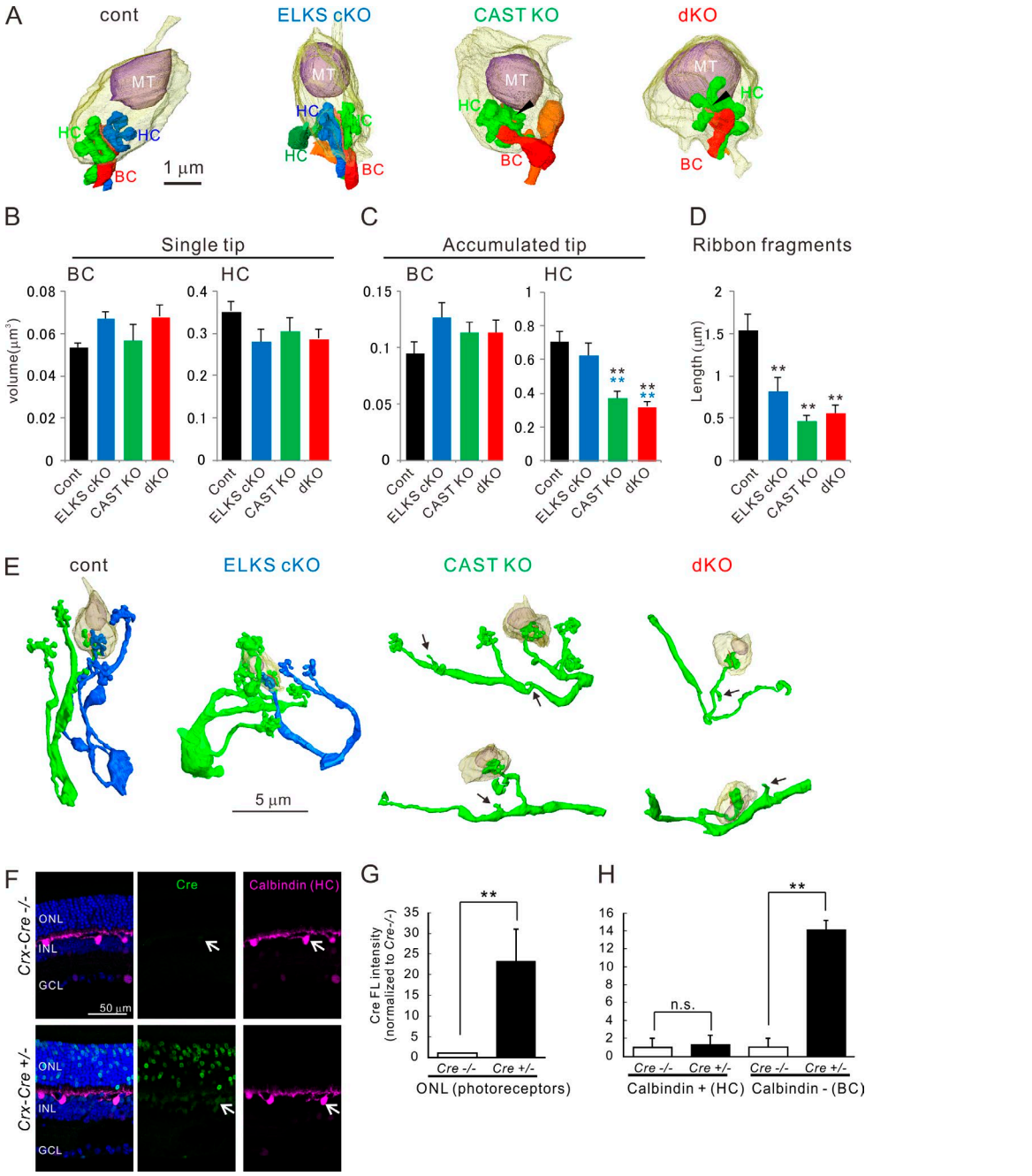

Figure S4. **3D reconstructed rod terminals and HC dendritic branching. (A)** Representative images of rod terminals of each genotype. Synaptic ribbons (pink bands) held by two horizontal tips (green and blue) in control and ELKS cKO, while the truncated ribbons were found in the single horizontal tip (green) in CAST KO and dKO (black arrowheads). The purple spherical object is mitochondria (MT). **(B–D)** The tip volumes of BC and HC of each single segment (B) and that were accumulated to compare them on each terminal (C). Since CAST KO and dKO possessed fewer HC tips, the accumulated HC volume of each terminal in CAST KO and dKO was almost half reduced compared to the control and ELKS cKO. Ribbon length of deletion mutants was significantly reduced compared to that of control (D). Mean ± SEM; data were collected from nine rod terminals, three rod terminals per each of three mice. **, P < 0.01 (one-way ANOVA followed by post hoc Tukey). **(E)** The HC tip which was composed triad in a rod terminal was further reconstructed to show its dendritic branching. In control and ELKS cKO, two HC tips (green and blue) demonstrated two independent branches consisting several branches and tips, which are assumed to inverted neighboring terminals. On the other hand, in CAST KO and dKO, a single HC tip (green) showed relatively sparse dendritic branching including little protrusions without tips (arrows). **(F)** Representative images of immunohistochemistry with anti-Cre (green) and anti-calbindin as the HC marker (magenta). Expression of Cre was recognized in the ONL and INL of *Crx-Cre*$^{+/-}$ retinae. Immunostaining for calbindin showed slight overlapping signal in the green channel (arrows). **(G and H)** Comparison of fluorescence (FL) intensity of Cre between *Crx-Cre*$^{-/-}$ and *Cre*$^{+/-}$ retinae. **(G)** Fluorescence intensity of Cre in *Cre*$^{+/-}$ photoreceptors was greater than that in *Cre*$^{-/-}$ photoreceptors, which were randomly picked by identification of DAPI signal in the ONL (n = 20 for each *Cre*$^{-/-}$ and *Cre*$^{+/-}$). Mean ± SEM; **, P < 0.01 (Student's t test). **(H)** In the INL, neurons were labeled by HC marker calbinding and divided into calbindin-positive (+) and -negative (–) cells. The fluorescence intensity of Cre was compared normalized to *Cre*$^{-/-}$ cells. The calbindin-positive HCs showed no significant increase of Cre expression, while calbindin-negative, mostly BCs showed increase of Cre expression. Mean ± SEM; n = 40 for each samples; **, P < 0.01 (one-way ANOVA followed by post hoc Tukey).

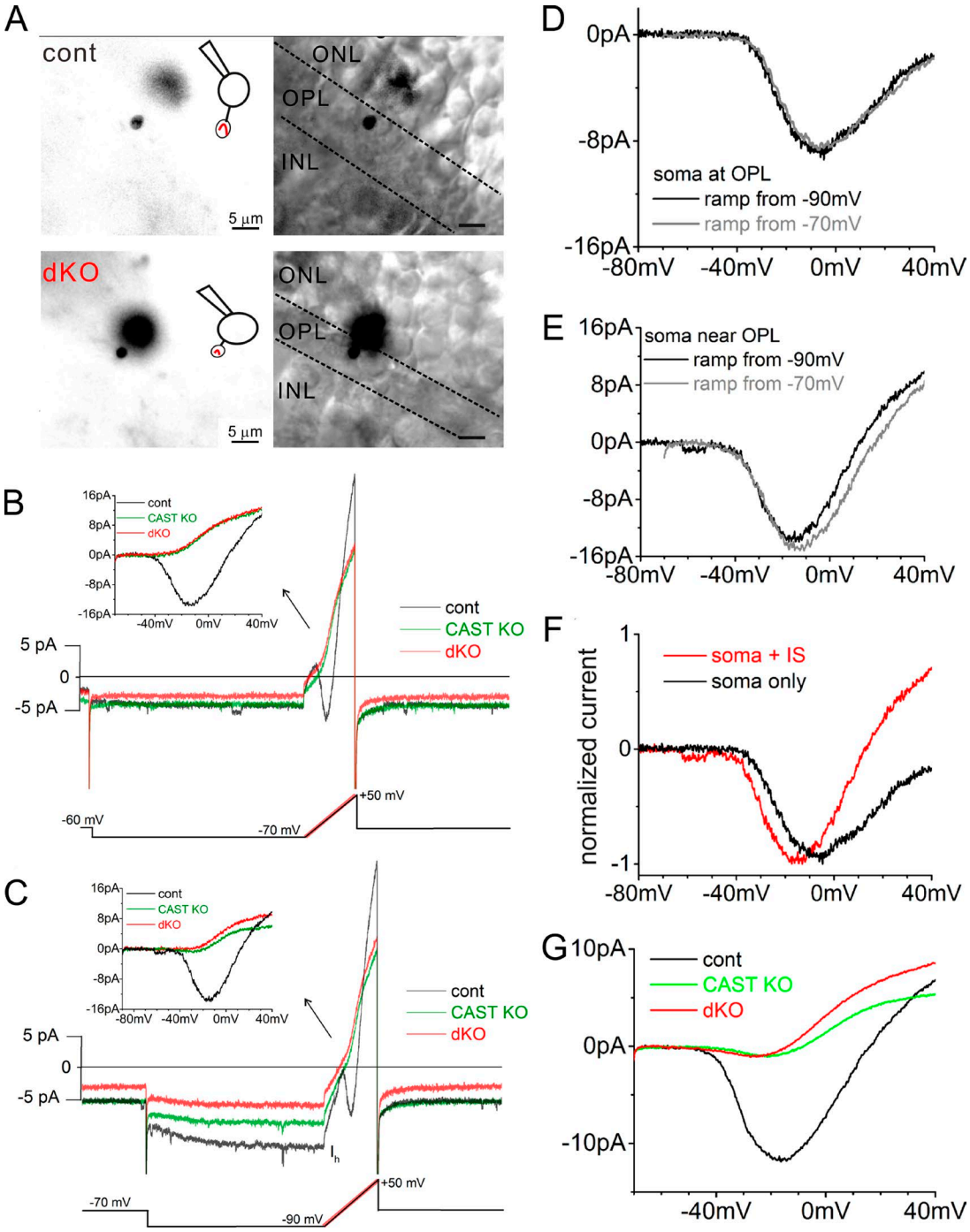

Figure S5. **Recording of Ca current from photoreceptor rods. (A–C)** Recording from the rod soma located several microns from the terminal. While all cells expressed I_h in C, which confirmed the intactness of recordings, the ramp portion of the protocol revealed that only the control showed the obvious inward I_{Ca}. The traces also showed that the additional cellular compartments (i.e., inner segment) created an outward current that appeared as the voltages rose above −20 mV. **(D and E)** Traces of I_{Ca} from control cells exhibiting ribbon synapses within the soma (D) or in the terminal (E). The traces indicate that the ramp protocol starting from −70 mV or −90 mV had less influence on the current. **(F)** Comparison of I_{Ca} traces from D and E (ramps started from −90 mV) illustrates that the soma at OPL (soma only) had much less outward current, corresponding to better voltage clamp. Even though the outward current tended to accelerate the activation of Ca_V channels, the peak amplitude of I_{Ca} was not significantly different (soma only, $V_{1/2}$ = −26 ± 0.8 mV, I_{Ca} = −14.5 ± 3.6 pA (n = 4); soma with inner segment (IS), $V_{1/2}$ = −31 ± 2.2 mV, I_{Ca} = −10.1 ± 3.1 pA (n = 5); P = 0.09 for $V_{1/2}$ and P = 0.5 for I_{Ca}). **(G)** Average I_{Ca} for the indicated genotypes. Traces are presented with 1 kHz low-pass filtering.

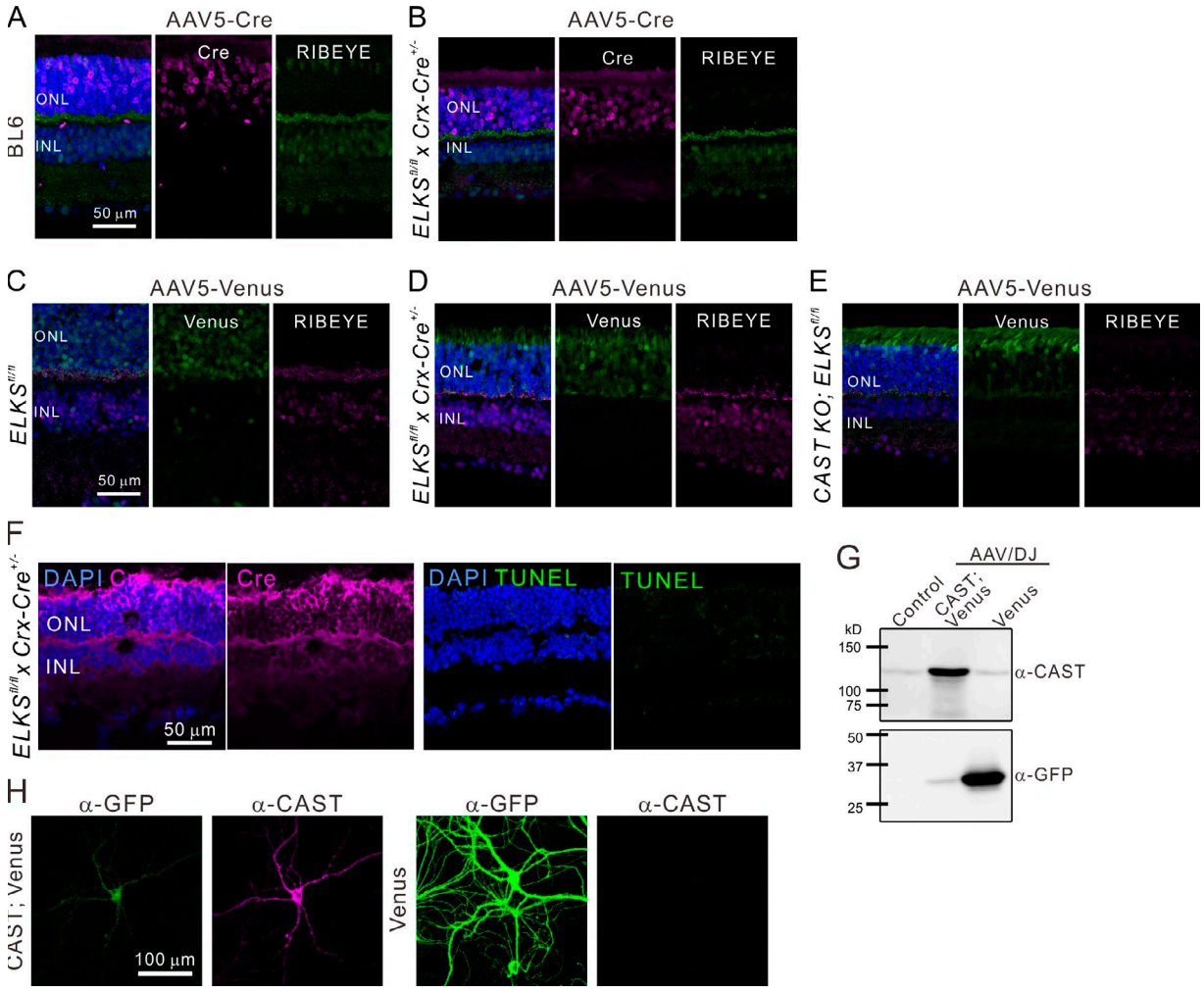

Figure S6. **AAV-mediated expression of Cre, Venus, and CAST-Venus in neurons. (A)** Injection of AAV5-CAGGS-nCre (AAV5-Cre) to the BL6 mouse retina showed expression of Cre recombinase in ONL without remodeling of photoreceptors and ribbon synapses labeled by RIBEYE. **(B)** In ELKS cKO (*ELKS*$^{fl/fl}$ *x Crx-Cre*$^{+/-}$), since Crx promoter–driven Cre recombinase has been eliminated, the expression of ELKS in photoreceptors during the development and the acute expression of Cre with AAV5 had not induced the photoreceptor remodeling. **(C–E)** Expression of Venus in *ELKS*$^{fl/fl}$ (C), *ELKS*$^{fl/fl}$ *x Crx-Cre*$^{+/-}$ (D), or *CAST KO; ELKS*$^{fl/fl}$ (E) mouse retina with AAV5 had less effect on photoreceptors and immunolabeling for RIBEYE. **(F)** Expression of Cre recombinase in ELKS cKO retina showed few TUNEL-positive photoreceptor neurons. **(G and H)** To confirm the AAV-mediated expression of CAST and Venus in neurons, AAV/DJ-CAGGS-CAST-IRES-Venus (CAST; Venus) and AAV/DJ-CAGGS-IRES-Venus (Venus) were infected into rat hippocampal primary culture neurons. Administration of AAV/DJ-CAST; Venus strongly enhanced the expression of CAST compared with control (non–AAV-treated) neurons, which contained endogenous CAST. While AAV/DJ-Venus caused strong expression of fluorescent protein detected by anti-GFP antibody, AAV for CAST-Venus was less effective in inducing Venus expression. Similar to the immunoblotting results, immunohistochemistry of primary culture neurons exhibited CAST expression with a weak Venus signal by the AAV/DJ-CAST-Venus. AAV/DJ-Venus showed a bright Venus signal.

Table S1. **Size of eyeball and ratio of protein concentration in retina**

	Size of eyeball			Protein concentration
	Width (mm)	**Depth (mm)**	***n***	**Ratio (% of control)**
Control	3.16 ± 0.03	3.21 ± 0.03	5	100 ± 0
ELKS cKO	3.20 ± 0.06	3.28 ± 0.05	7	97.5 ± 3.4
CAST KO	3.18 ± 0.04	3.11 ± 0.03	5	92.5 ± 2.9
dKO	3.07 ± 0.05	3.03 ± 0.03[a]	5	81.7 ±1.9[b,c]

Values for size of eyeballs are means ± SEM. Protein concentrations from retinal homogynates were measured with the Bradford assay. Values are means ± SEM, n = 5.
[a]P < 0.01 versus ELKS cKO (one-way ANOVA followed by Tukey test)
[b]P < 0.01 versus Cont and ELKS cKO.
[c]P < 0.05 versus CAST KO (one-way ANOVA followed by Tukey test).

Table S2. **Volumes of each structure from 3D-reconstructed rod terminals**

Volume	**Rod terminal (µm³)**	**Mitochondria (µm³)**
Control	8.29 ± 0.38 (9)	1.99 ± 0.17 (9)
ELKS cKO	8.10 ± 0.22 (9)	1.66 ± 0.11 (9)
CAST KO	7.91 ± 0.29 (9)	1.86 ± 0.17 (9)
dKO	8.07 ± 0.63 (9)	1.50 ± 0.24 (9)
	BC tip (µm³)	
	Single	Accumulated
Control	0.054 ± 0.002 (16)	0.095 ± 0.009 (9)
ELKS cKO	0.067 ± 0.003 (17)	0.127 ± 0.013 (9)
CAST KO	0.057 ± 0.008 (18)	0.114 ± 0.008 (9)
dKO	0.068 ± 0.006 (15)	0.114 ± 0.011 (9)
	HC tip (µm³)	
	Single	Accumulated
Control	0.353 ± 0.024 (18)	0.706 ± 0.058 (9)
ELKS cKO	0.280 ± 0.030 (20)	0.623 ± 0.075 (9)
CAST KO	0.305 ± 0.033 (11)	0.372 ± 0.036 (9)[ab]
dKO	0.287 ± 0.022 (10)	0.319 ± 0.033 (9)[a,b]

Values are means ± SEM. Data were collected from nine terminals, three terminals per each of three mice, and averaged from indicated sample numbers in parentheses.
[a]P < 0.01 versus control.
[b]P < 0.01 versus ELKS cKO (one-way ANOVA followed by Tukey test).

Table S3. **Surface areas of each structure from 3D-reconstructed rod terminals**

Surface area	**BC (µm²)**		**HC (µm²)**	
	Single	Accumulated	Single	Accumulated
Control	1.08 ± 0.04 (16)	1.91 ± 0.15 (9)	6.16 ± 0.23 (18)	12.32 ± 0.40 (9)
ELKS cKO	1.37 ± 0.07 (17)	2.59 ± 0.23 (9)	5.17 ± 0.53 (20)	11.48 ± 1.32 (9)
CAST KO	1.11 ± 0.11 (18)	2.21 ± 0.15 (9)	5.90 ± 0.53 (11)	7.21 ± 0.63 (9)[a,b]
dKO	1.50 ± 0.19 (15)	2.24 ± 0.25 (9)	5.98 ± 0.33 (10)	6.41 ± 0.49 (9)[a,b]

Values are means ± SEM. Data were collected from nine terminals, three terminals per each of three mice, and averaged from indicated sample numbers in parentheses. The horizontal surface areas of each terminal in CAST KO and dKO were significantly decreased from control and ELKS cKO.
[a]P < 0.01 versus control.
[b]P < 0.01 versus ELKS cKO (one-way ANOVA followed by Tukey test).

Table S4. **Ratio of fragmented ribbons**

	Ratio of fragmented ribbons
Control	1/9 (11%)
ELKS cKO	4/9 (44%)
CAST KO	2/9 (22%)
dKO	3/9 (33%)

Data were collected from nine terminals, three terminals per each of three mice. We found one of nine ribbons in Cont broken up in two, probably because of technical artifact of less contrast of ribbon in scanning EM. However, in other mutant retina, more ribbons were found in two pieces, especially in ELKS cKO. Though deletion of ELKS seemed to have little effect on retinal morphology and function, the ELKS might have a role on the structural basis of ribbon synapse.

Table S5. **HC line density**

	Line density (cells/mm)	*n*
Control	22.0 ± 5.7	4
ELKS cKO	18.6 ± 6.0	4
CAST KO	22.4 ± 3.0	5
dKO	21.2 ± 4.9	4

Values are means ± SEM. The HCs were immunolabeled with anti-calbindin antibody and detected by the HRP method.

Table S6. **Statistical analysis**

Figure	Statistical test	F	P value
Fig. 1 E, Western blot			
ELKS	One-way ANOVA	F (3, 20) = 34.8	3.9.E-08
CAST	One-way ANOVA	F (3, 12) = 108.7	5.8.E-09
RIM1/2	One-way ANOVA	F (3, 8) = 23.8	2.4.E-04
Fig. 1 H, b-wave			
Interaction	Two-way ANOVA	F (18, 138) = 20.6	<0.0001
Intensity factor	Two-way ANOVA	F (6, 138) = 237.4	<0.0001
Genotype factor	Two-way ANOVA	F (3, 23) = 25.4	<0.0001
Fig. 1 I, oscillatory potential			
Interaction	Two-way ANOVA	F (18, 138) = 9.4	<0.0001
Intensity factor	Two-way ANOVA	F (6, 138) = 151.8	<0.0001
Genotype factor	Two-way ANOVA	F (3, 23) = 12.6	<0.0001
Fig. 2 C			
Interaction	Two-way ANOVA	F (24, 153) = 2.9	<0.0001
Distance factor	Two-way ANOVA	F (8, 153) = 179.9	<0.0001
Genotype factor	Two-way ANOVA	F (3, 153) = 40.7	<0.0001
Fig. 2 D, Control			
Interaction	Two-way ANOVA	F (12, 42) = 0.15	1.000
Distance factor	Two-way ANOVA	F (6, 42) = 184.5	<0.0001
Age factor	Two-way ANOVA	F (2, 42) = 0.021	0.979
Fig. 2 D, CAST KO			
Interaction	Two-way ANOVA	F (24, 135) = 2.2	3.0.E-03
Distance factor	Two-way ANOVA	F (8, 135) = 209.7	<0.0001
Age factor	Two-way ANOVA	F (3, 135) = 26.3	<0.0001
Fig. 2 D, dKO			
Interaction	Two-way ANOVA	F (24, 135) = 3.0	<0.0001
Distance factor	Two-way ANOVA	F (8, 135) = 132.9	<0.0001
Age factor	Two-way ANOVA	F (3, 135) = 57.8	<0.0001
Fig. 3, A–C			
OPL, ONL	One-way ANOVA	F (3, 17) = 8.5	1.1.E-03
ONL	One-way ANOVA	F (3, 17) = 27.0	1.1.E-06
OPL	One-way ANOVA	F (3, 17) = 24.2	2.3.E-06
Fig. 3 E			
Rod terminal density	One-way ANOVA	F (3, 86) = 38.6	6.9.E-16
Fig. 3 G			
Docked vesicle	One-way ANOVA	F (3, 17) = 3.6	3.6.E-02
Fig. 4, D–F			
BC	One-way ANOVA	F (3, 32) = 0.7	0.558
HC	One-way ANOVA	F (3, 32) = 22.1	6.0.E-08
HC surface	One-way ANOVA	F (3, 32) = 13.9	5.5.E-06
Fig. 4, G and H			
Ribbon length	One-way ANOVA	F (3, 32) = 17.6	6.4.E-07
Distance	One-way ANOVA	F (3, 32) = 3.4	0.029
Fig. 5, I_{Ca}			
Control, CAST KO	Two-sided *t* test	t (15) = −4.3	6.7E-4

Table S6. **Statistical analysis *(Continued)***

Figure	Statistical test	F	P value
Control, dKO	Two-sided *t* test	t (23) = −6.2	2.7E-6
CAST KO, dKO	Two-sided *t* test	t (22) = −0.34	0.74
Fig. 6 E, ONL			
ELKS fl, Cre	Two-sided *t* test	t (8) = 2.3	0.047
ELKS fl, Venus	Two-sided *t* test	t (2) = −0.2	0.836
ELKS cKO, Cre	Two-sided *t* test	t (4) = 0.9	0.417
ELKS cKO, Venus	Two-sided *t* test	t (4) = 1.9	0.133
CAST KO; ELKS fl, Cre	Two-sided *t* test	t (4) = 3.9	0.017
CAST KO; ELKS fl, Venus	Two-sided *t* test	t (4) = 1.2	0.298
Fig. 6 F, RIBEYE			
ELKS fl, Cre	Two-sided *t* test	t (8) = 3.0	0.018
ELKS fl, Venus	Two-sided *t* test	t (2) = −0.2	0.833
ELKS cKO, Cre	Two-sided *t* test	t (4) = 2.4	0.075
ELKS cKO, Venus	Two-sided *t* test	t (2) = 2.5	0.132
CAST KO; ELKS fl, Cre	Two-sided *t* test	t (6) = 7.4	3.1.E-04
CAST KO; ELKS fl, Venus	Two-sided *t* test	t (4) = 0.5	0.629
Fig. 7, C and E			
CAST-Venus	Two-sided *t* test	t (35) = 0.02	0.985
Venus	Two-sided *t* test	t (24) = 4.8	6.6.E-05
Fig. S2 A, male			
Interaction	Two-way ANOVA	F (30, 1084) = 1.4	0.072
Time factor	Two-way ANOVA	F (10, 1084) = 588.6	<0.0001
Genotype factor	Two-way ANOVA	F (3, 1084) = 115.0	<0.0001
Fig. S2 A, female			
Interaction	Two-way ANOVA	F (24, 732) = 1.6	0.034
Time factor	Two-way ANOVA	F (8, 732) = 250.6	<0.0001
Genotype factor	Two-way ANOVA	F (3, 732) = 56.9	<0.0001
Fig. S2 G			
Whole	One-way ANOVA	F (3, 8) = 3.4	0.070
ONL	One-way ANOVA	F (3, 8) = 2.2	0.164
OPL	One-way ANOVA	F (3, 8) = 17.0	8.E-04
INL	One-way ANOVA	F (3, 8) = 2.6	0.126
IPL	One-way ANOVA	F (3, 8) = 4.4	0.042
Fig. S2 H			
ONL	One-way ANOVA	F (3, 8) = 1.7	0.241
INL	One-way ANOVA	F (3, 8) = 1.5	0.292
Fig. S4, B–D			
Single tip volume, BC	One-way ANOVA	F (3, 62) = 1.9	0.146
Single tip volume, HC	One-way ANOVA	F (3, 55) = 1.5	0.226
Accumulated volume, BC	One-way ANOVA	F (3, 32) = 1.5	0.221
Accumulated volume, HC	One-way ANOVA	F (3, 32) = 12.5	1.4.E-05
Ribbon length	One-way ANOVA	F (3, 42) = 11.8	9.4.E-06
Fig. S4, G and H			
ONL	Two-sided *t* test	t (38) = −2.8	0.008
INL	One-way ANOVA	F (3, 156) = 137.6	<0.0001